JOURNAL OF GEOPHYSICAL RESEARCH, VOL. 114, C05019, doi:10.1029/2008JC005165, 2009

On the spreading of South Atlantic Water into the Northern Hemisphere

Kerstin Kirchner,[1] Monika Rhein,[1] Sabine Hüttl-Kabus,[1] and Claus W. Böning[2]

Received 22 October 2008; revised 23 February 2009; accepted 12 March 2009; published 19 May 2009.

[1] The upper branch of the meridional overturning circulation in the North Atlantic is fed by cross-equatorial transport of various water masses from the Southern Hemisphere. Here, we study the large-scale spreading of South Atlantic Water (SAW) into the western tropical North Atlantic from the equator to 25°N. The fractions of SAW in the upper ocean water masses are quantified using a water mass analysis applied on a data set of conductivity-temperature-depth data from the Hydrobase project and the Argo float program. To fill gaps in the data coverage and to gain insight into the mechanisms involved, the observations are complemented with results from the high-resolution Family of Linked Atlantic Model Experiments model ($\frac{1}{12}°$), which has been shown to realistically simulate the inflow of SAW into the Caribbean. The analysis reveals the mean SAW propagation pathways in the North Atlantic and identifies the regions of largest variability. High SAW fractions in the thermocline and central water layers are limited to the region south of 10°N, where the water body consists of 80%–90% SAW. Thus, the zonal currents in the equatorial gyre are mainly formed of SAW. The weaker currents in the intermediate layer combined with a northward excursion of the North Equatorial Current allow the SAW in this layer to intrude farther north compared to the layers above. The transition into North Atlantic Water occurs gradually from 12°N to 20°N in the intermediate layer.

Citation: Kirchner, K., M. Rhein, S. Hüttl-Kabus, and C. W. Böning (2009), On the spreading of South Atlantic Water into the Northern Hemisphere, *J. Geophys. Res.*, *114*, C05019, doi:10.1029/2008JC005165.

1. Introduction

[2] The current system of the upper tropical Atlantic Ocean (the water column from the surface to approx. 1100 m) consists of two components, which closely interact with each other: (1) several zonal current bands, which possess only limited meridional and vertical extents, and (2) superimposed on the zonal currents is the upper limb of the meridional overturning circulation (MOC), which creates a net northward volume and heat transport in the tropical Atlantic. The resulting current system is characterized by an intense northward western boundary current and alternating zonal flows in the interior Atlantic, which are connected by shallow meridional cells (STCs and TCs) [see *Zhang et al.*, 2003; *Fratantoni et al.*, 2000]. An extensive presentation of the equatorial currents is given by *Stramma et al.* [2003] or by *Schott et al.* [1998] for the western tropical Atlantic, here we will constrain ourselves to an overview of the flows relevant for this study.

[3] Westward currents in the tropical North Atlantic are the northern branch of the South Equatorial Current (SEC) and the North Equatorial Current (NEC) (Figure 1), which are part of the southern and northern subtropical gyres. The broad and sluggish SEC and NEC transport water masses from the eastern subtropics toward the west within several current branches. The topographic conditions allow the NEC to continue unhindered to 60°W, where it encounters the Antilles Islands, partly enters the Caribbean or deflects northwestward. The SEC is blocked by the South American coastline at 40°W, where it bifurcates into a southern and a northern current off Brazil [*Stramma and Schott*, 1999]. The northern component actually continues into the North Atlantic as the North Brazil Current (NBC). The behavior of the subtropical gyres on the equatorial edge is thus asymmetric in the Atlantic.

[4] Near 5°N the surface intensified North Equatorial Countercurrent (NECC) flows eastward, while subsurface (eastward) cores are found in the Equatorial Undercurrent (EUC), which is located directly at the equator, and the North Equatorial Undercurrent (NEUC) at 3°N (see *Brandt et al.* [2006] for details). These surface and subsurface currents are schematically depicted in Figure 1, as well as the topographic conditions in the western tropical North Atlantic. The upper ocean current system in the tropical Atlantic shows a strong seasonal signal [e.g., *Schott et al.*, 1998]; especially the position of the NBC retroflection and the surface NECC are subjects of high variability.

[5] In the intermediate layer (400–1100 m depth), the currents partly reverse: Below the EUC the Equatorial

[1]Institut für Umweltphysik, Abteilung Ozeanographie, Universität Bremen, Bremen, Germany.
[2]Leibniz Institut für Meereswissenschaften an der Universität Kiel (IFM-GEOMAR), Kiel, Germany.

0148-0227/09/2008JC005165$09.00

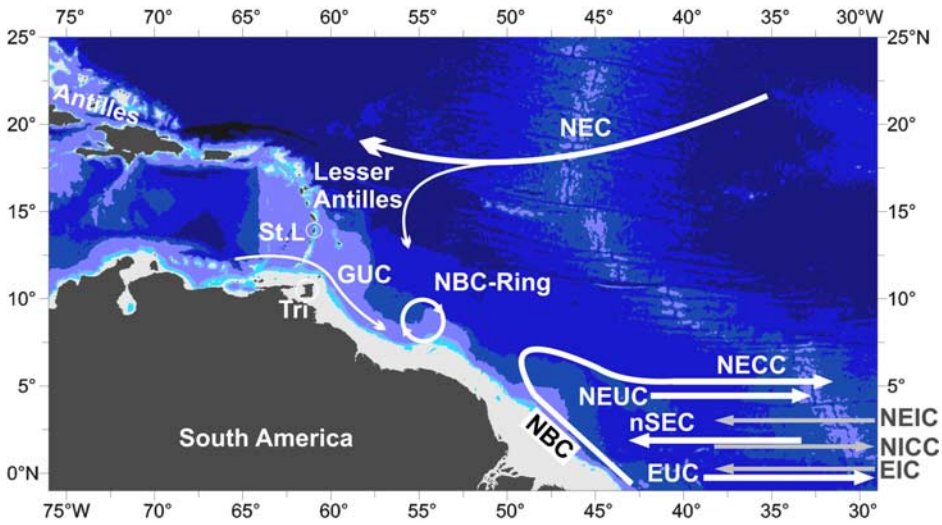

Figure 1. The topography of the western tropical North Atlantic with a schematic overview of the circulation pattern. Surface and thermocline intensified currents are depicted in white, and intermediate currents are depicted in gray. NEC, North Equatorial Current; GUC, Guyana Undercurrent (thermocline); NBC, North Brazil Current; NECC, North Equatorial Countercurrent; NEUC, North Equatorial Undercurrent (thermocline); nSEC, South Equatorial Current (northern branch); EUC, Equatorial Undercurrent (thermocline); NEIC, North Equatorial Intermediate Current; NICC, Northern Intermediate Countercurrent; EIC, Equatorial Intermediate Current; St.L, St. Lucia; Tri, Trinidad.

Intermediate Current (EIC) flows from east to west [*Brandt et al.*, 2008]. Off the equator every 2° in latitude, altering zonal jets are found as well, such as the Northern Intermediate Countercurrent (NICC) and the North Equatorial Intermediate Current (NEIC), which are discussed by *Ollitrault et al.* [2006] and indicated in Figure 1.

[6] The cross-hemispheric transport within the NBC brings upper ocean water masses from the Southern Hemisphere into the North Atlantic. The NBC feeds the EUC and retroflects eastward near 7°N into the NECC, the major part of its water thus recirculates in the equatorial gyre. Northern hemispheric waters may contribute to the EUC and NECC via recirculations of the NEC or the Guyana Undercurrent (GUC), which has been reported to flow out of the Caribbean Sea along the South American coast toward the equator [*Bourles et al.*, 1999b; *Fratantoni et al.*, 2000]. *Zhang et al.* [2003] used historical ADCP data to estimate the relatively small transport of the boundary pathway of North Atlantic water into the equatorial region.

[7] The equatorial gyre is fed heterogeneously: the inflow of southern water masses dominates the near-equatorial water body. Modeling studies suggest that this asymmetry is a result of the MOC influence on the current system [*Jochum and Malanotte-Rizzoli*, 2003; *Fratantoni et al.*, 2000]. Furthermore, large eddies develop at the retroflection (so called NBC rings), which are associated with the interhemispheric MOC transport [*Garzoli et al.*, 2003]. No marked seasonality was found in the ring shedding [*Goni and Johns*, 2003; *Fratantoni and Glickson*, 2002]. While propagating northwestward, the rings conserve the unique South Atlantic Water (SAW) features in their core and may reach the Lesser Antilles [e.g., *Fratantoni and Glickson*, 2002]. They were observed by *Rhein et al.* [2005] even farther north. Hence the transition region between water masses of northern and southern hemispheric origin in the tropical Atlantic is situated well north of the equator, but its position and structure is still unknown and a topic of this work. We focus our study on the mean state of the circulation and the water masses; and present results obtained from an averaged hydrographic data set of profiles, which were accumulated during the last 15 years.

[8] The SAW remaining in the North Atlantic feeds into the Florida Current [*Schmitz and Richardson*, 1991] and presents an important contribution to the meridional overturning in the Atlantic. Here, we examine the mean spreading of SAW into the Northern Hemisphere for a data set of observed hydrographic data, as well as modeling results from the high-resolution (Family of Linked Atlantic Model Experiments (FLAME)) model. We identify the transition zone of the domain dominated by southern hemispheric waters to northern waters and outline the regions of largest water mass variability. While the strong contribution of SAW to the equatorial currents was already discussed in earlier publications [e.g., *Schott et al.*, 1998; *Bourles et al.*, 1999b], we now calculate and quantify the SAW in the northern equatorial currents (such as the NEUC and NEIC). The identification of the fractions of SAW was done by a water mass analysis with temperature and salinity, using an isopycnal mixing approach. We discuss the results in detail and the implications for the equatorial current system are pointed out using the modeled velocity field in FLAME.

1.1. Water Masses

[9] The water masses relevant for this study form the water column from the surface to about 1200 m (the density σ_θ = 27.6 kg m^{-3}) in the tropical Atlantic. The characterization of the water masses and their limiting densities are chosen according to the regime in the western tropical North Atlantic, following the description by *Stramma and Schott* [1999], and used by *Rhein et al.* [2005] and *Kirchner et al.* [2008, Figure 2].

[10] The warm and thin surface layer and the underlying high-salinity layer are known as Tropical Surface Water (TSW; $\sigma_\theta < 24.5$ kg m^{-3}) and Salinity Maximum Water (SMW) ($\sigma_\theta = 24.5–26.3$ kg m^{-3}). TSW occupies the upper 50 m to 80 m of the tropical Atlantic. It is modified by the atmosphere and river input, especially by the Amazon River outflow near the equator and the Orinoco plume at 8°N. θ-S analyses are invalid for surface water, thus we exclude TSW from our analysis and restrain this work to the water masses below. The northward transport of equatorial TSW was already analyzed by *Signorini et al.* [1999] with Chlorophyll a distributions or by *Hellweger and Gordon* [2002], who tracked the low-salinity signature of the Amazon outflow to Barbados. A discussion of the surface currents in the western tropical Atlantic and the Caribbean Sea can be found in the paper by *Cherubin and Richardson* [2007] as well.

[11] The SMW layer is characterized by high salinity and warm temperatures [*Mémery et al.*, 2000]. In both hemispheres this highly saline water mass is formed by the excess of evaporation over precipitation in the subtropics and advected westward within the subtropical gyre. Some works name these waters Subtropical Underwater (SUW), since the distinct salinity core is found at about 100 m depth [e.g., *Goes et al.*, 2005]. The northern salinity maximum lies in the density range bounded by the 25.6 kg m^{-3} to 26.3 kg m^{-3} isopycnals [*Snowden and Molinari*, 2003]. The salinity in this layer exceeds 37 psu in the formation region; near the Lesser Antilles the salinity in northern SMW is still higher than in southern SMW and the maximum is found at a slightly higher density than its southern counterpart (σ_θ = 25.5 kg m^{-3} versus σ_θ = 25.0 kg m^{-3}) [*Bourles et al.*, 1999a].

[12] The South Atlantic provides a second source in the density range of SMW, which is noticeably fresher [*Wilson et al.*, 1994]. From the eastern South Atlantic, this water mass (denoted East Atlantic Water, EAW, [e.g., *Bourles et al.*, 1999a]) is brought to the western boundary with the equatorial branch of the SEC. When crossing the equator, the SMW layer within the NBC consists of both southern sources. In contrast, the NEC carries only salty water in this density range [*Wilson et al.*, 1994]. The θ-S properties of the high-salinity waters are similar for both the northern and the southern type, leading to a failure of a θ-S water mass analysis. Therefore this work will focus on the fresher, eastern South Atlantic source, namely the EAW, assuming that this source represents most of the South Atlantic contribution to the SMW layer. The error made by this assumption and the possible contribution of the salty western South Atlantic source to the SMW layer will be discussed in the Conclusions.

[13] The third layer is formed by Central Water (CW) (σ_θ = 26.3–27.1 kg m^{-3}). The Central Waters are characterized by an almost linear θ-S relationship; the northern CW is found at higher salinities than the southern type. The CW is further subdivided into an upper and a lower part (UCW and LCW) by the isopycnal σ_θ = 26.8 kg m^{-3} (similar to *Rhein et al.* [2005]). South of 15°N, the South Atlantic Central Water (SACW) was found to dominate this layer [*Klein and Tomczak*, 1994].

[14] Intermediate Water (IW) (σ_θ = 27.1–27.8 kg m^{-3}) is the deepest layer considered in this work. This layer is dominated by inflow from the south, consisting of Antarctic Intermediate Water (AAIW). The salinity minimum within the AAIW can be traced best at the western boundary, into the Caribbean Sea and to 24°N [*Suga and Talley*, 1995].

1.2. Research Area

[15] This work focusses on the western tropical Atlantic, namely the region from the equator to 25°N and from 30°W to 75°W. Since the strongest cross hemispheric current is the NBC at the western boundary, the investigation is targeted to this area. The restriction of the area matches the limits of the water mass analysis as well (see section 2.3): isopycnal mixing is only a valid assumption near the western boundary. Within the subtropical/tropical cells in the interior Atlantic vertical movements (upwelling, downwelling) are enhanced and diapycnal mixing is not negligible. Farther east of 30°W the STCs prohibits a hydrographic tracking of the SAW and a water mass analysis cannot be applied there. The defined source waters border the area of investigation to the north and south. Only the northern SMW source at 16°N lies inside this area, since the North Atlantic SMW subducts south of 25°N.

2. Data and Methods

2.1. Data Set of Argo Profiles and CTD Data

[16] Ship cruises carried out by the University of Bremen [*Rhein et al.*, 2005] and data provided by HydroBase [*Curry*, 2001] for the western tropical North Atlantic yield together 1833 temperature and salinity profiles for the western tropical North Atlantic, obtained from 1993 to 2005. While this appears to be a considerable quantity of profiles, they were all gained during short periods, which often repeated earlier sections. The data resolution is therefore more than sufficient in some regions and very poor in other regions. To increase the data coverage, the conductivity-temperature-depth (CTD) data is complemented with Argo profiles. Argo profiles are freely available on the websites of the Argo Data Centers (e.g., http://www.coriolis.eu.org/). For the defined domain Argo provides more than 10,000 profiles in the period January 2000 to June 2007. However, many of them do not contain information on salinity and thus cannot be used for the water mass analysis (see section 2.3), or exhibit other problems.

[17] For the analysis, all available T/S Argo profiles were used, including real-time data provided by the Argo Data Centers. While the delayed mode profiles can be considered carefully checked by the distributing institutions, the real time data often need additional, careful inspection. An extended quality control was developed to avoid false results through not validated profiles (on the basis of the Argo quality control manual: http://www.coriolis.eu.org//cdc/argo/argo-quality-control-manual.pdf). The following quality checks were implemented:

[18] 1. All profiles that were marked as erroneous by the Global Data Assembly Centers (GDAC) were filtered out.

[19] 2. All profiles which were taken by floats listed on the grey list provided by the GDACs (e.g., floats with sensor malfunctions) were filtered out.

[20] 3. Suspicious data for the considered region in the tropical North Atlantic were removed (e.g., salinities above 41).

[21] 4. Density increasing with depth was checked, and density inversions were erased.

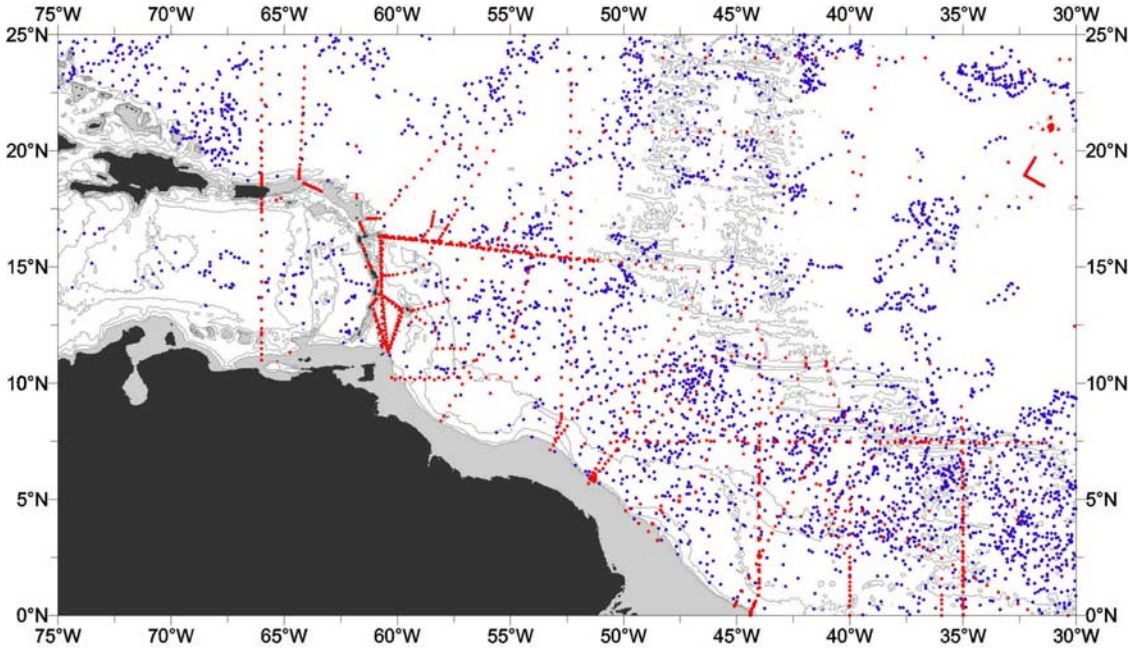

Figure 2. Locations of quality-checked profiles, obtained by Argo floats (blue) and ship measurements (red) from 1993 to 2007. The shelf shallower than 500 m is shaded in gray, and the 1000 m, 2000 m, and 4000 m isobaths are indicated.

[22] 5. A statistical scan was performed. The data set was divided into regional boxes, containing 10°–20° in latitude and longitude. The mean profile was calculated for every box, and single profiles varying more than the doubled standard deviation from the mean were removed.

[23] By this approach the data were filtered thoroughly; but the possibility of remaining systematic errors, like sensor drift, cannot be ruled out. In total, 3171 Argo profiles with salinity data passed the test. Combined with shipboard CTD profiles, 5004 T/S profiles were available, the locations are presented in Figure 2, where the Argo profiles are indicated in blue and the CTD stations in red. The distribution of the profiles is irregular in space and time, and is insufficient to resolve seasonal or interannual signals over the whole domain. Therefore, our results depict a mean situation of the SAW distribution, obtained by hydrographic measurements from 1993 to 2005.

2.2. Model

[24] The analysis of SAW spreading is complemented by results from a general circulation ocean model. The high-resolution model FLAME [*Dengg et al.*, 1999] has been developed at IFM-GEOMAR in Kiel for studying the wind-driven and thermohaline circulation in the Atlantic Ocean and meets the demands necessary for this study [*Kirchner et al.*, 2008]. FLAME is based on the Modular Ocean Model code (MOM2.1) [*Pacanowski*, 1995], solving the primitive equations, but several refinements were applied to the configuration [*Eden and Böning*, 2002].

[25] The spin-up of the model starts from a climatology based on a combination of *Levitus and Boyer* [1994] and *Boyer and Levitus* [1997] and is sufficiently long for an adjustment of dynamical processes in the thermocline. The MOC reaches a first quasi-equilibrium, i.e., MOC drift becomes small. There is no significant MOC drift over the analysis period (it is clear that a MOC drift does not vanish completely: this would require integration times of O(1000 years), but inevitably lead to model states with unrealistic water mass properties). The model is forced with monthly mean wind stresses and a linearized bulk formulation for heat fluxes based on a climatology of the European Centre for Medium Range Forecasts (ECMWF) analysis following *Barnier et al.* [1995] and the DYNAMO study [*Willebrand et al.*, 2001]. The model uses a rigid lid as upper boundary and the surface salinity was relaxed to the Levitus climatology on a timescale of 30 days. In coastal areas this relaxation implicitly includes the effects of river runoffs, manifested in low-salinity caps near, e.g., the Amazon and Congo. The northern and southern boundaries are open boundaries with climatological inflow conditions for temperature and salinity and vertically integrated transports from an Arctic model [*Brauch and Gerdes*, 2005] at the northern boundary. The southern boundary condition is calculated from the Sverdrup relation and the combined Levitus climatology. Sea surface salinity is damped toward this climatology as well. Vertical mixing is parameterized on the basis of a stability-dependent scheme for vertical diffusivity and viscosity [*Böning and Kröger*, 2005], and a KT scheme [*Kraus and Turner*, 1967] for the mixed layer. The model uses biharmonic friction and Laplacian isopycnal diffusion [cf. *Hüttl-Kabus and Böning*, 2008].

[26] The simulation considered here uses a horizontal grid of $\frac{1}{12}^\circ$ and 45 vertical levels, for a domain from 70°N to 18°S in the Atlantic [cf. *Böning et al.*, 2006]. The model has been integrated for 9 years with climatological forcing; the results in this study are based on the last year of this climatological run. The results of *Hüttl and Böning* [2006] showed, that the $\frac{1}{12}^\circ$ version of FLAME realistically reproduces the zonal current bands near the equator, in contrast to the $\frac{1}{3}^\circ$ version. *Kirchner et al.* [2008] used combined model

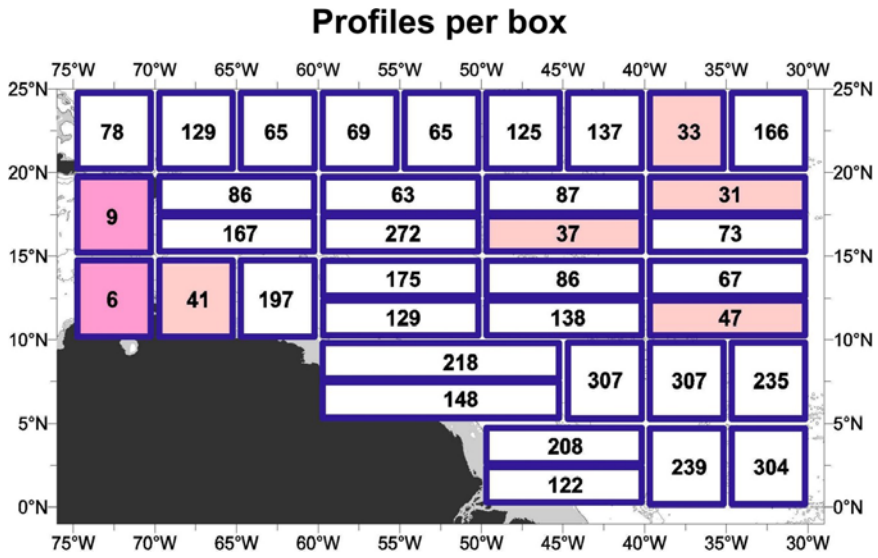

Figure 3. Choice of subdomains with number of quality-proved profiles available in each box. Boxes with less than 50 and 10 profiles are shaded light and dark pink, respectively.

and observation results to discuss the inflow of SAW into the Caribbean. They pointed out, that FLAME reproduces the tropical water masses satisfyingly and is suitable for applications in the tropical North Atlantic.

2.3. Water Mass Analysis

[27] We applied a water mass analysis using an isopycnal mixing approach, where salinity and temperature data are taken as constraints. The θ-S analysis is used to calculate the portion of SAW within the water column (measured or modeled). For defining the sources, which are considered to be representatives of the pure northern and southern waters, profiles from historical CTD data in the North and South Atlantic were chosen [*Rhein et al.*, 2005]. The analysis calculates the fraction of each source component necessary to obtain the properties of the given water sample. The result is the SAW fraction in percent. The method is applied to the water column from $\sigma_\theta = 24.5$ kg m^{-3} to $\sigma_\theta = 27.6$ kg m^{-3}. The model simulates the observed water masses very accurately [*Kirchner et al.*, 2008] and the same separating isopycnals and source water positions are used as in the observational analysis.

[28] At each hydrographic station (or model grid point) the respective SAW fractions in the water column were calculated. The overall error of the water mass fractions are ±6% in the Central Waters, and ±12% for the SMW and IW and include uncertainties due to the choice of the θ-S characteristics of source water masses and diapycnal mixing.

[29] The results for the SMW north of 16°N must be handled with care, since the SMW source water masses were defined at 16°N, south of the subduction region. That is, however, not the case for the deeper layers (Central and Intermediate Waters). The method is described in detail by *Rhein et al.* [2005] and was used by *Kirchner et al.* [2008] as well (potential temperature/salinity plots are given in these papers). We point out again, that the salty South Atlantic SMW source is not covered by the analysis, as well as the surface water above $\sigma_\theta = 24.5$ kg m^{-3}, although these waters also contribute to the northward transport of SAW. An estimate of the importance of the salty, western SMW source is given in the conclusions.

2.4. Choice of Subdomains

[30] The observations over the whole time period were merged and averaged over subdomains. The shape, orientation and horizontal extent of the geographical boxes were chosen to minimize the standard deviation (STD in the following) of the mean SAW fraction of all four water masses within a box (the resulting boxes or subdomains are illustrated in Figure 3). The analysis was started with regular 5° × 5° boxes, which exhibited high STDs. By altering the shape and orientation of the boxes, we found the presented composition of subdomains with lowest possible STDs. The remaining areas of high STD reflect either variability of the water mass composition due to unresolved temporal or interannual processes, or the high STDs are caused by strong gradients of SAW content at the transition zone from SAW to North Atlantic Water (NAW). A possible meandering of the transition zone may also result in elevated STDs. The mainly zonal alignment of the boxes follows the orientation of the circulation scheme described in the introduction.

[31] Almost every box contains more than 50 quality-proved profiles, only five exhibit a lower accumulation of 30–50 profiles (shaded boxes in Figure 3). The western Caribbean is badly sampled with less than 10 profiles. Results based on data from these boxes should be handled with caution.

3. Results

3.1. Large-Scale SAW Distribution From Observations

[32] The mean SAW fractions for each box and the corresponding standard deviations are depicted in Figures 4 and 5. Apparently, SAW dominates the region south of 10°N, where the fractions reach 50%–100% in all density layers. Farther north, the regime changes to North Atlantic water mass dominance. North of 20°N the contribution of SAW has decreased to less than 20%. Figures 4 and 5 particularly highlight the strong South Atlantic contribution

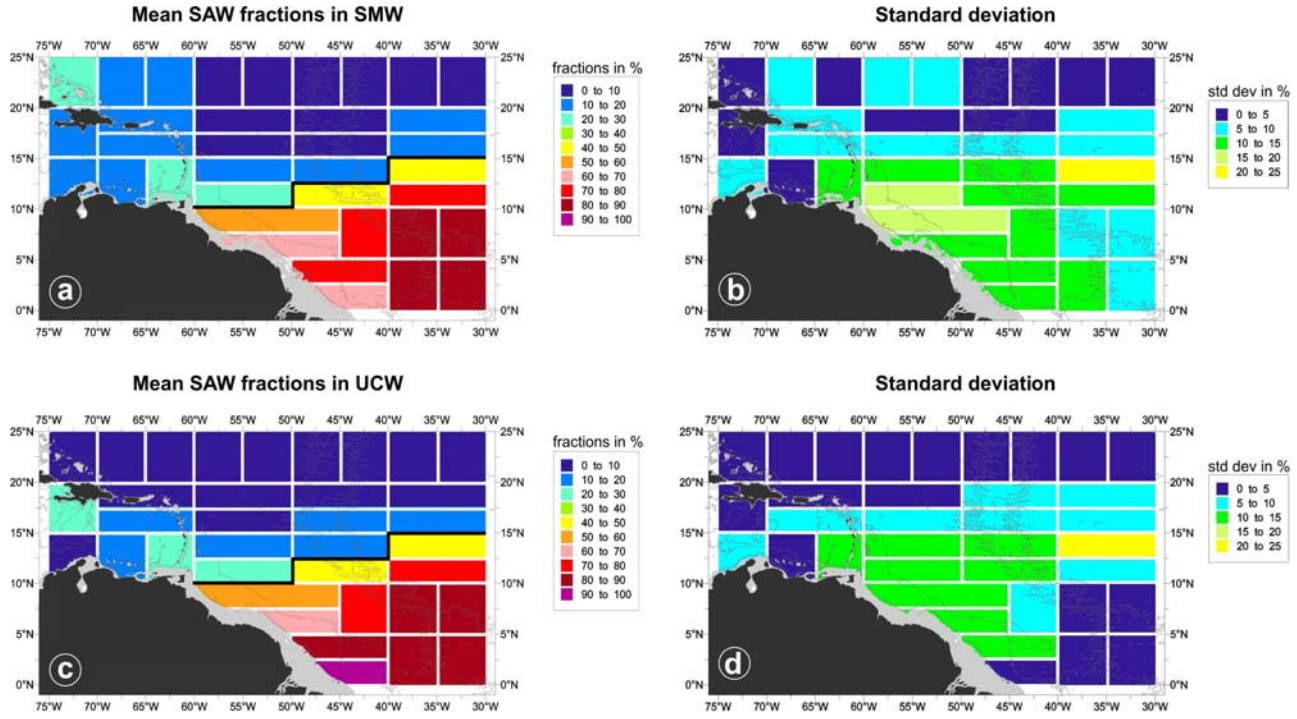

Figure 4. Mean South Atlantic Water distribution (percent) in the western tropical North Atlantic. (a) SAW distribution in SMW, (b) corresponding standard deviation, (c) SAW distribution in UCW, and (d) corresponding standard deviation. The shelf shallower than 100 m is shaded in gray in Figures 4a and 4b, and the shelf shallower than 200 m is shaded in gray in Figures 4c and 4d. The black lines in Figures 4a and 4c indicate the strongest meridional decrease of SAW at the transition region from SAW to NAW. Note the different color scales.

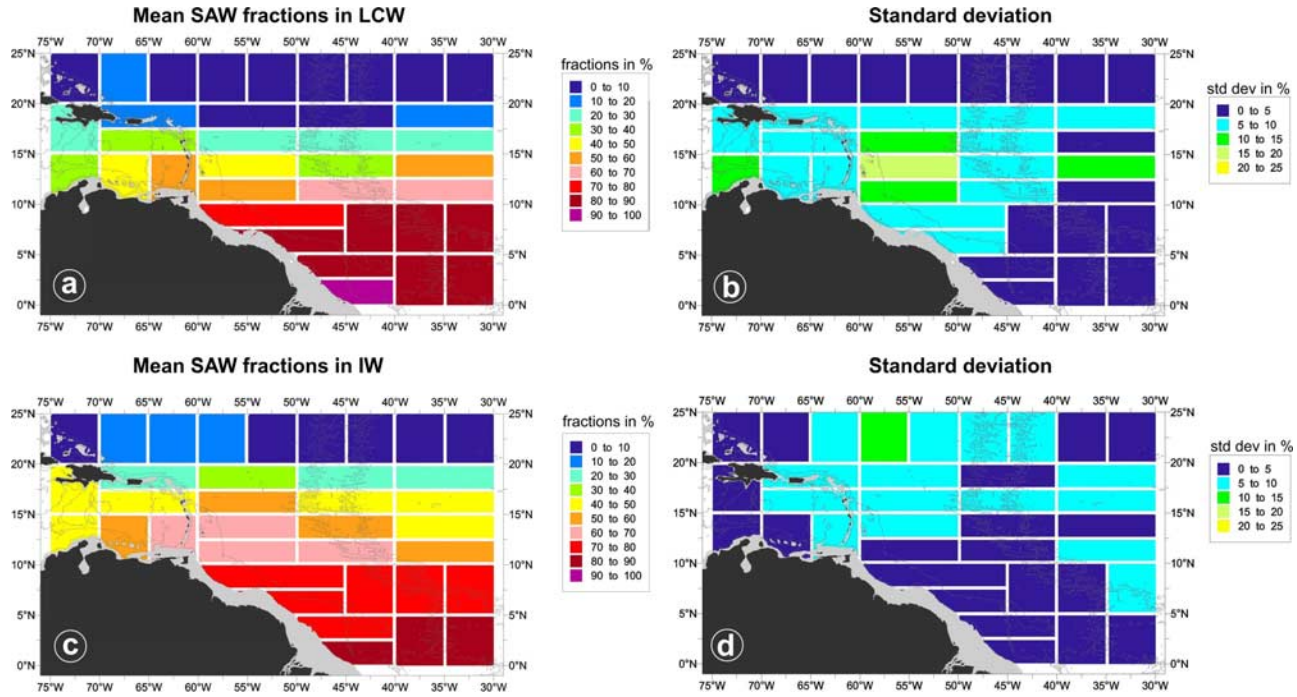

Figure 5. Mean South Atlantic Water distribution (in percent) in the western tropical North Atlantic. (a) SAW distribution in LCW, (b) corresponding standard deviation, (c) SAW distribution in IW, and (d) corresponding standard deviation. The shelf shallower than 200 m is shaded in gray in Figures 5a and 5b, and the shelf shallower than 500 m is shaded in gray in Figures 5c and 5d. The transition region from SAW to NAW is broader and zonal in these density layers and thus not indicated in these layers (contrary to Figure 4). Note the different color scales.

to the water masses of the equatorial current system in the Atlantic (cf. *Stramma and Schott* [1999] or Figure 1).

[33] The maximum percentage of SAW in the water masses is highest in the Central Water; both the upper and lower CW contain 90%–100% of SACW off the Brazilian shelf near the equator (Figures 4c and 5a). The area from the equator to 10°N and from 30°W to 40°W reveals 80%–90% of SAW in all layers, only the AAIW influence slightly decreases in the northern boxes.

[34] The Caribbean Sea exhibits the strongest SAW influence in the southeast. The box contains the southern Lesser Antilles Islands and thus the passages, which were found to be of major importance for the SAW inflow into the Caribbean [*Kirchner et al.*, 2008]. From south to north, the SAW fractions in the LCW and IW decrease inside the Caribbean Sea. The island arc forms a barrier, the transport into the Caribbean occurs mainly in the southern passages. West of 70°W, the IW layer still consists of more than 40% SAW in the Caribbean Sea.

[35] The transition region from southern hemispheric water to NAW is found to be staggered in the different density layers. The upper two layers (SMW and UCW) (Figures 4a and 4c) both exhibit a sharp decrease in SAW fractions at a bordering line from near Trinidad to 15°N, 30°W. The abrupt decline in SAW fractions is indicated by the black lines in Figures 4a and 4c, where a strong meridional gradient of 20%–30% decrease in SAW content occurs. South of this zonally inclined border the SAW fractions are at least 40% (up to 100%). North of this border SAW percentages above 20% are present only in the southeastern Caribbean, the water column is mainly formed of NAW in this region. The changes occur on a narrow spatial scale (maximum 5°), especially east of 50°W, and thus lead to high variability within the affected boxes. Consequently, the STD is elevated along the encountered boundary of SAW influence (illustrated in Figures 4b and 4d), which is caused by the crossover from high SAW fractions to low SAW fractions in this region.

[36] Although NBC rings are known to propagate farther north than 10°N along the island arc of the Lesser Antilles [*Rhein et al.*, 2005], or to disintegrate at the southern passages [*Fratantoni and Richardson*, 2006], no prominent SAW signal at the Lesser Antilles in the SMW and UCW layers is evident. The SAW fractions in these layers were found to be 30%–37% at the Lesser Antilles [*Rhein et al.*, 2005], that is 10%–30% less than in the LCW and IW layers. The mean ring volume transport in the SMW and UCW is thus too small to produce a strong SAW signal for the defined subdomain. Nevertheless, we find regions of high STD grouped at the South American coast and the southern Lesser Antilles Islands, where rings propagate northwestward [e.g., *Fratantoni and Glickson*, 2002]. Hence we conclude that the high STDs in this region are most likely produced by NBC rings, which transport high SAW anomalies in their center and thus generate variability along the western boundary. The NBC retroflection, which sheds the rings, alters its position between 5°N and 10°N [*Johns et al.*, 1990] and thus provides another source for elevated STDs at the western boundary.

[37] High SAW contributions reach noticeably higher latitudes in the two lower layers (LCW and IW). As illustrated in Figures 5a and 5c the transition region from SAW to NAW stretches from 12°N to 18°N in the LCW and is not declined. The strong spatial gradient of SAW content found in the upper layers is missing (hence Figure 5 contains no black line). While the SAW fractions in the equatorial North Atlantic (south of 7°N) are similarly high in UCW and LCW, the propagation of UCW is clearly inhibited compared to LCW. The recirculation within the equatorial gyre is thus less important in the LCW layer than in the UCW, where the recirculation restricts the spreading of SAW.

[38] The SAW distribution in the IW layer is not much different from the LCW, but SAW influence is evident to 20°N and even north of this latitude between 70°W and 55°W. The distribution is smooth and the SAW influence gradually decreases, not as abrupt as in the upper layers. The zonal equatorial currents (EIC, NICC, NEIC) in the IW layer lay well within the influence zone of AAIW and exhibit only minor contributions from the northern hemispheric waters.

[39] The standard deviation for the two lower layers (Figures 5b and 5d) is generally smaller than the STD for the upper layers (compare Figures 4b and 4d with Figures 5b and 5d). The LCW exhibits high variability off the Lesser Antilles, at 60°W to 50°W. The NBC rings, which do not enter the Caribbean Sea, possibly pass within this corridor. From shipboard measurements at 16°N, *Rhein et al.* [2005] identified several NBC rings in the Atlantic east of the island arc, which for the most part showed small SAW percentages in SMW and UCW, but large SAW fractions in the LCW and IW.

[40] The described SAW distribution indicates a major recirculation of SMW and UCW within the equatorial gyre into the NECC and NEUC. In Figure 4 no prominent influence of the GUC is apparent. South Atlantic Waters dominate the coastal region south of 10°N and only small NAW contributions to the NEUC and EUC are found. In the lower layers (LCW and IW) (Figure 5) SAW spreads evenly to latitudes farther north, which points to a minor role of equatorial recirculation for the water mass spreading and less interaction with the NEC. In the next section we will use the model results to investigate the connection between the SAW distribution and the current field near the NBC retroflection and farther north.

3.2. Large-Scale SAW Distribution in the FLAME Model

[41] The large-scale water mass distribution in FLAME was investigated with the same methods as the observational data. The model analysis covers the area from 5°N to 24°N and from 30°W to 70°W. We use the annual mean data sets from the climatological run, which are suitable for a direct comparison of the results obtained by the observational data set. The annual mean SAW fractions were calculated and the distribution is illustrated in Figure 6 for all four water masses, as well as the corresponding standard deviation. Additionally, the annual mean currents in the respective layers are shown in Figure 7. The velocity field was averaged to an annual mean as well, and while it is sufficient to depict the mean state of the currents, short-term fluctuations (such as individual NBC rings) are not resolved.

[42] The main features of the current field (cf. Figure 1 versus Figure 7) are evident in the modeled velocity

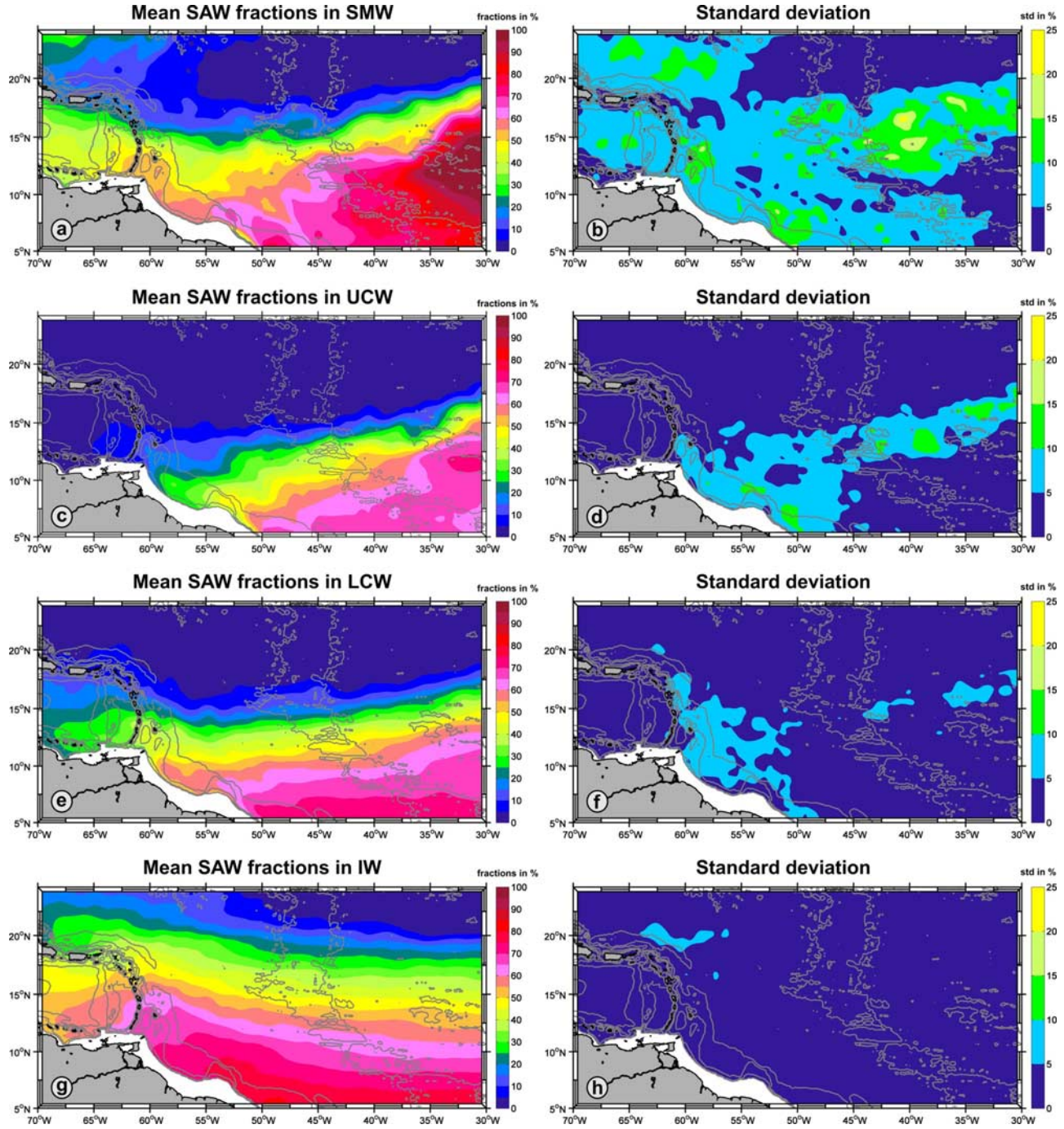

Figure 6. Mean South Atlantic Water distribution (in percent) in the western tropical North Atlantic in FLAME. (a) Annual mean SAW distribution in SMW, (b) corresponding standard deviation, (c) annual mean SAW distribution in UCW, (d) corresponding standard deviation, (e) annual mean SAW distribution in LCW, (f) corresponding standard deviation, (g) annual mean SAW distribution in IW, and (h) corresponding standard deviation. Note the different color scales.

throughout the water column and highlighted (red vectors) in Figure 7: The NBC is crossing the equator at the western boundary (feature 1) and the retroflection feeds the NECC/NEUC (feature 2). The NEC forms a broad, mainly westward current band centered at 20°N (feature 3). The connection from the retroflection toward the Caribbean Sea (feature 4) is formed by a prominent current along the shelf in the annual mean current field, resulting from NBC rings averaged with background currents.

[43] The transition region from southern hemispheric waters to NAW is different in each modeled water mass. In the SMW layer high South Atlantic contributions are found south of 12°N (>50%) and near the Lesser Antilles south of St. Lucia (Figure 6a). The transition region from SAW to NAW gets sharper in the east: east of 45°W a

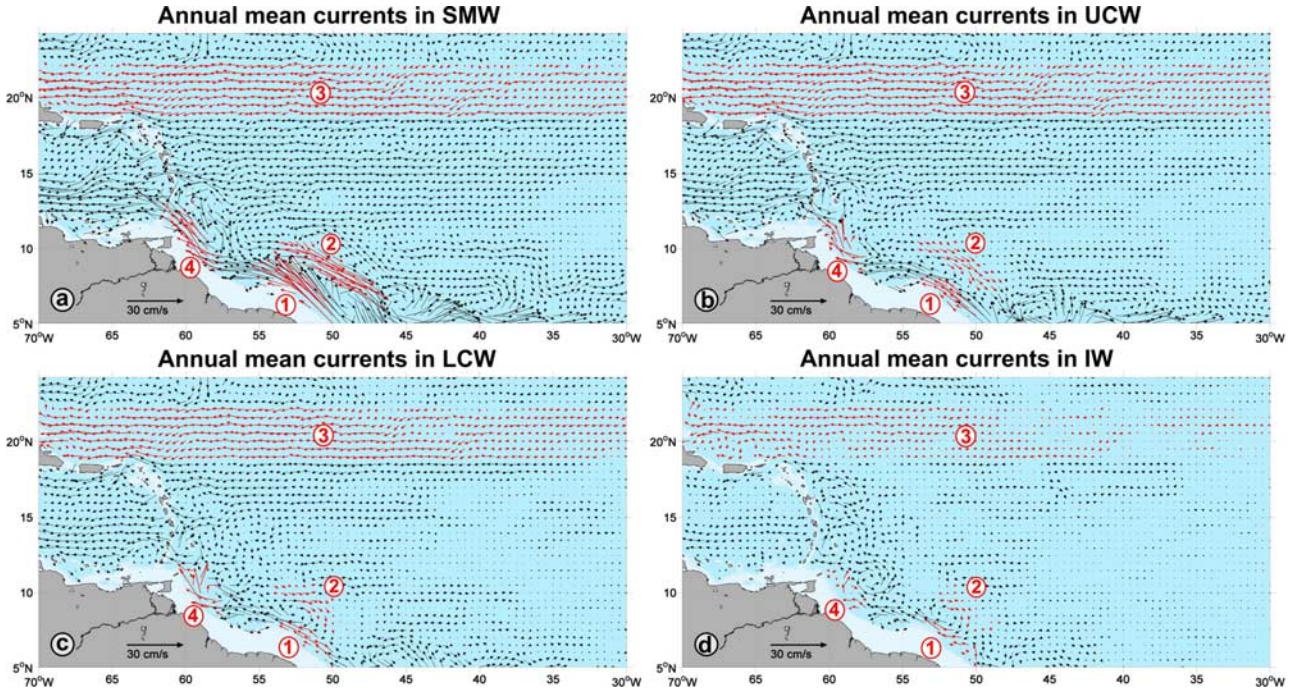

Figure 7. Annual mean currents in FLAME. (a) SMW layer, (b) UCW layer, (c) LCW layer, and (d) IW layer. Some features in the current field are highlighted with numbers and red vectors: feature 1 (NBC), feature 2 (NECC), feature 3 (NEC), and feature 4 (transport toward the Caribbean). The velocity resolution in Figure 7 was reduced to $\frac{1}{2}^\circ$ for clarity.

distinct front of SAW can be seen. The transition front is inclined, analog to the observational results. Near the Lesser Antilles the front is found at 12°N, while at our easternmost position at 30°W the latitude of transition is 17°N. The southern SMW enters the Caribbean Sea and is still noticeable at 70°W throughout the Caribbean. The standard deviation shows variability of mainly 5%–15% for the SMW (Figure 6b), indicating prevalent variations in this water mass. At the transition region, where the water mass properties change on a small spatial scale, the STD is highest. The annual mean currents are illustrated in Figure 7a, where the resolution was reduced to enhance the clarity (to $\frac{1}{2}^\circ$). The NEC (feature 3) is evident to 15°N east of the Lesser Antilles and transports NAW into the northern Caribbean. The coastal current near South America (feature 4) brings southern SMW into the Caribbean Sea and along the island arc as far as St. Lucia. Near the islands the currents are disturbed by the topography and form small-scale gyres. The velocity is highest in the NBC, where the current speed exceeds 45 cm s^{-1}. No GUC is evident in the mean velocity field in FLAME.

[44] The Central Waters exhibit a reduced northward spreading of SAW (Figures 6c and 6e) compared to the SMW layer, strong South Atlantic influence is only evident south of 7°N for the UCW and south of 10°N for the LCW layer at the western boundary. The transition region is inclined again: the front of SAW is found at 15°N at 30°W. North of 20°N the SAW fractions are below 5% in both CW layers. Elevated STDs (Figures 6d and 6f) are similarly distributed: at the shelf south of 10°N for the UCW layer and at the Lesser Antilles for the LCW layer, then following the transition front. However, the variability in the LCW layer is much weaker than in the layers above.

[45] Additionally, elevated STDs are found in the UCW layer (Figure 6d) along the South American coastline and at the Lesser Antilles south of St. Lucia. NBC rings occasionally carry high amounts of SAW in the UCW layer to the Lesser Antilles, and the modeled current field is reproducing this behavior. Since the SAW transport within the rings is too small to increase the mean SAW fractions north of Trinidad above 20%, only the high standard deviation denotes this disturbances. This interpretation holds as well for the LCW layer in Figures 6e and 6f along the island arc of the Lesser Antilles. Incidental transport along the island arc north of 15°N is indicated by the STD. While the southern origin LCW contributes slightly to the Caribbean inflow, the SAW fractions in the UCW do not indicate a significant transport into the Caribbean. The mean velocity field in the UCW layer (Figure 7b) is congruent with the SMW velocities, but for the southeastern area from 12°N, 60°W. The currents in the NBC (feature 1) are noticeably weaker (<20 cm s^{-1}) and the retroflection into the NEUC (feature 2) only slightly reduced, thus the major SAW portion recirculates in the equatorial gyre. The Caribbean inflow at the southern passages is weak. The northward current along the South American coastline (feature 4) is influenced by a zonal flow from the east, which leads to entrainment of NAW. The farther spreading of LCW compared to the UCW can be explained by a weaker recirculation into the NEUC, and the lower SAW fractions within the NBC in the UCW layer. Furthermore, the NEC in the LCW layer is weakened south of 17°N, forming small-scale recirculations and hence weakening the NAW transport. In

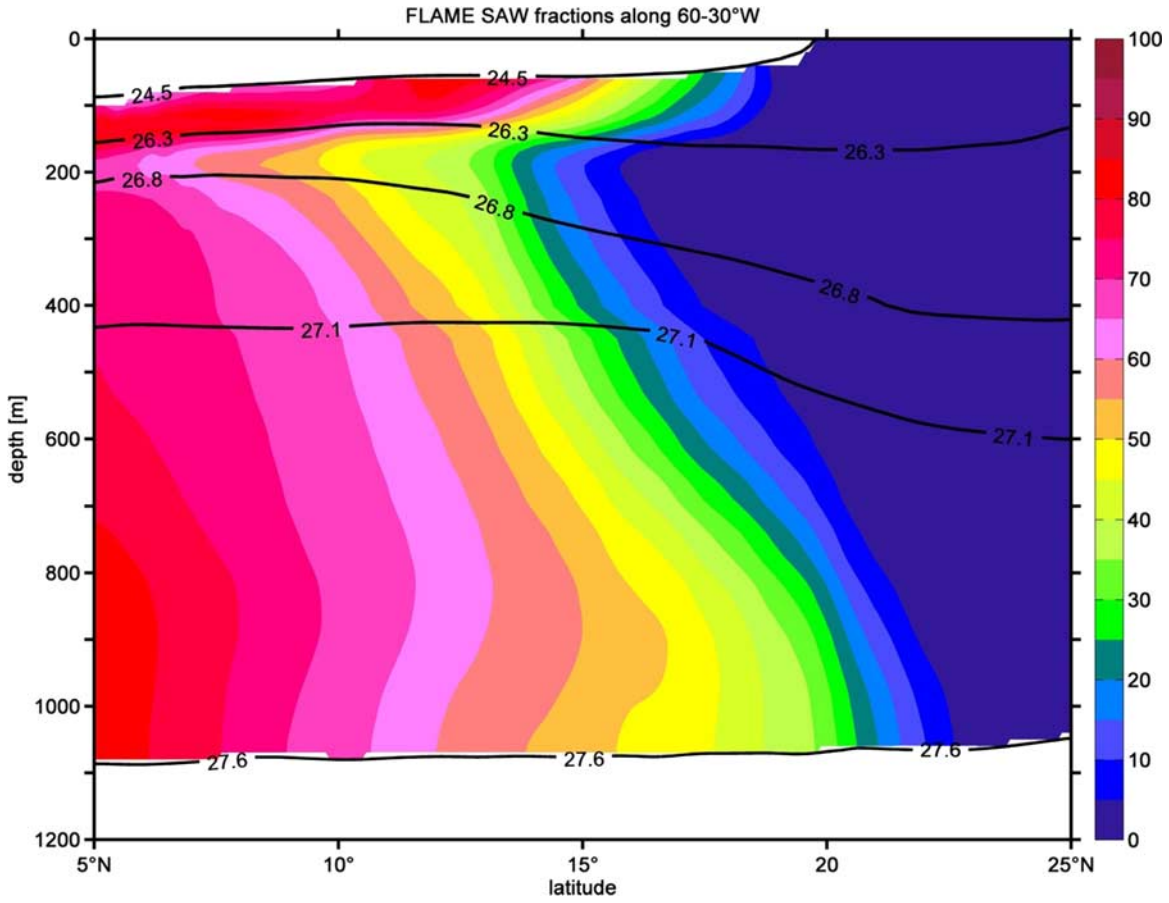

Figure 8. Mean vertical SAW distribution (in percent) in the zonal band 30–60°W from 5°N to 25°N. The bordering isopycnals, which confine the water mass layers, are depicted in black.

contrast, strong NEC currents are evident in the UCW layer from 14°N northward (cf. Figures 7b and 7c).

[46] The most extensive northward spreading of SAW is evident in the IW layer, as shown in Figure 6g. In the intermediate depth, the transition region from SAW to NAW is found at 13°–17°N. The southern IW does not only spread into the Caribbean, but also along the island arc on the Atlantic side of the Lesser Antilles. The transition of southern IW (namely AAIW) to North Atlantic IW occurs gradually and equally in the west and east, since no inclined transition zone occurs. At 5°N the contribution of southern IW to the intermediate layer exceeds 75%. The currents in the equatorial system (EIC, NICC, NEIC) are thus formed mainly of AAIW in the model, consistently to the observational results. The IW layer exhibits very small variability, only at the transition region north of 18°N elevated STDs are present (Figure 6h). The variability in the Caribbean Sea is remarkably low, indicating a continuous supply of SAW passing into the Caribbean in this layer. Considering the velocity field (Figure 7d), a further reduction of the strength and extension of the NEC (feature 3) is evident. Only north of 20°N a continuous westward flow is found, hence the supply of NAW to the southern latitudes of the Lesser Antilles is reduced. Recirculation into the equatorial region (feature 2) is insignificant for the water mass spreading in this layer.

[47] The different meridional spreading of SAW in the density layers is illustrated in Figure 8. Depicted are the mean SAW fractions for the zonal band 30°–60°W along 5°–25°N. High SAW fractions of more than 70% at the southern end of the section are evident in all layers, but the northward spreading shows a distinct minimum in the UCW at 13°N.

4. Summary and Conclusions

[48] The large-scale distribution of SAW was investigated by hydrographic ship measurements, profiles from Argo floats and modeling results. The SAW fractions were calculated by a water mass analysis using temperature and salinity information. The analysis revealed the mean SAW spreading into the North Atlantic and thereby identified the ring translation corridor along the South American coast as the region of largest variability. The same analysis was applied on model data from the high-resolution ocean model FLAME, where the velocity field was used to interpret the water mass spreading. The mean SAW distribution in the FLAME model agrees in the general features with the observational results.

[49] SAW was found to dominate the region east of 60°W and south of 10°N in the observational analysis, here mean SAW fractions reached 50%–100% in all density layers. The area south of 10°N from 30°W to 40°W consists of 80%–90% SAW in the SMW and Central Water layers. The areas directly located at the western boundary contain even higher SAW fractions in the Central Water, but slightly

lower fractions in the SMW. We gain the following conclusions from this distribution of SAW: the fresh EAW dominates the equatorial region and thus impedes the northward spreading of the southwestern salty SMW source (cf. section 1.1). The EAW is brought to the western boundary by the central and northern branches of the SEC (evident in the high fraction from 30° to 40°W, south of 10°N in Figure 4a), while the salty southern SMW is concentrated near the coast. In the boxes south of 5°N, between 40°W and the coast both water masses mix and are advected northward within the NBC. The salty SMW can contribute at maximum 30% to the water body of the SMW in the NBC, since EAW already contributes 70%–80% at 5°–10°N. Assuming that the main sources for the northward transport out of the tropical gyre are located at the western boundary, namely within the NBC and its rings, we conclude that the salty SMW therefore is not as important for the MOC as the fresher EAW. Furthermore, our results show that the water masses transported by the equatorial currents (namely the NEUC, and the deeper parts of the NECC and EUC) essentially contain SAW, at least in the density range below σ_θ = 24.5 kg m^{-3}, which is the upper boundary of our analysis, the contribution of NAW to these currents is restricted to 0%–20%.

[50] The spreading of South Atlantic SMW is slightly enhanced in the model, compared to the observations. For the Central Water, observations and model agree on a low spreading of southern UCW into the Northern Hemisphere, but the model indicates generally less SAW fractions in both CW layers than the observations. Presumably these water masses recirculate into the equatorial gyre in the model too strongly, while the recirculation of SMW into the NECC is weaker than indicated by observations. Using Lagrangian float analysis, *Hüttl-Kabus and Böning* [2008] already showed that in FLAME the major water body within the off-equatorial undercurrents is formed of SAW, corresponding to our results. This finding agrees as well with *Schmitz and Richardson* [1991], who reported a low contribution of South Atlantic thermocline water to the Caribbean inflow and the Florida current.

[51] Whether a continuous GUC exists cannot be clarified by this work. However, we conclude that the southward transport of North Atlantic Water within the GUC or recirculating NEC branches is small for latitudes south of 7°–5°N, justified by the water mass distribution in both the observational analysis and FLAME. In the model no mean southward Undercurrent is present, but the inclined transition region may indicate a southward transport of NAW along the western boundary. It is worth mentioning that the existence of the GUC was first noted in model simulations characterized by a very weak MOC in the tropical Atlantic [*Schott and Böning*, 1991]. Accordingly, the GUC in FLAME is either a weak and variable current, or interacting with the northward drifting NBC rings and thus contains some amount of SAW as well. Its contribution to the NEUC and EUC is therefore of low NAW signature. The seasonal variability of the equatorial current system seems to have no impact on the water mass distribution. STDs south of 5°N are low in all density layers (cf. Figures 4 and 5). Likewise no marked seasonal cycle in the formation of NBC rings was found [*Goni and Johns*, 2003].

[52] The agreement between the SAW distribution obtained by observations and the FLAME model is best in the IW layer. The SAW distribution is smooth and the AAIW influence gradually decreases from south to north. AAIW spreads farthest into the North Atlantic and a moderate transition into NAW is found from 12°N to 20°N. At the equator the AAIW dominates the water body (80%–90% SAW) and thus forms the EIC and the NICC/NEIC.

[53] The transition region from SAW to NAW is zonally inclined in the observational analysis of the upper two layers (SMW and UCW), extending from Trinidad to 15°N, 30°W. This behavior was reproduced by the climatological run with FLAME. *Stramma et al.* [2005] describe a secondary core of the NECC between 8° and 10°N at 24°W in observations and FLAME, called nNECC. They found a strong exchange between the nNECC and the NECC/NEUC. The northern core of the NECC was noted by *Urbano et al.* [2008] as well between 9° and 15°N farther west, during measurements at the PIRATA mooring position at 38°W. They found a meandering NECC and two cores developing when the ITCZ reaches its northernmost location. The northern NECC was partly fed by waters from the Northern Hemisphere. The zonally inclined transition region for the SMW and UCW layers in our analysis may well be a feature of the second NECC core. Further work is needed to validate this point, for example model results with variability in the atmospheric forcing could yield valuable information.

[54] In the lower layers (LCW and IW), both observations and model reveal a more uniform spreading of SAW with stretched transition zones (small or no declination) from 12°N to 18°N for the LCW and to 20°N for the IW. On the locations of all transition regions elevated standard deviations are present. They indicate variability in the position of the transition zones: they may migrate northward and southward. Between 15°N and 20°N all South Atlantic water masses encounter the NEC (FLAME results, Figure 7), which is part of the North Atlantic subtropical gyre, and transports NAW westward. The NEC is weakest in the IW layer, suggesting that the sluggish northward flow of AAIW is not significantly disturbed by the NEC and thus leads to a uniform spreading to higher northern latitudes than possible for the upper layers. The salinity at 25°N on the σ_θ = 27.4 kg m^{-3} surface decreases from east to west in the observations (not shown), indicating an influence of low-saline AAIW from 58°W westward in the NEC.

[55] Currently, the spatial and temporal resolution in Argo and CTD data is not extensive enough to allow for analyzing seasonal changes or interannual variability. The Argo program shows promise in providing these data in the future. One aim will be to improve the resolution of the observational analysis and identify the areas of water mass variability in more detail and to validate the mean values in the regions with low data resolution. A separation into seasons would be the next step, when sufficient data coverage is available for all seasons. A similar analysis regarding seasonality and variability is planned with model data, on the basis of a model run including interannual variability.

[56] **Acknowledgments.** The data were partly collected and made freely available by the International Argo Project and the national programs that contribute to it (http://www.argo.ucsd.edu, http://argo.jcommops.org). Argo is a pilot program of the Global Ocean Observing System. We thank the Deutsche Bundesministerium für Bildung und Forschung (BMBF) and the Deutsche Forschungsgemeinschaft (DFG) for financial support. We

acknowledge the contributions of J. Dengg, R. Redler, J.-O. Beismann, C. Eden, and L. Czeschel to the FLAME development and integration. The computations were performed at DKRZ, Hamburg. We thank the two anonymous reviewers for their suggestions, which helped to improve the paper.

References

Barnier, B., L. Siefridt, and P. Marchesiello (1995), Thermal forcing for a global ocean circulation model using a three-year climatology of ECMWF analysis, *J. Mar. Syst.*, *6*, 363–380.

Böning, C., and J. Kröger (2005), Seasonal variability of deep currents in the equatorial Atlantic: A model study, *Deep Sea Res., Part I*, *52*, 99–121.

Böning, C., M. Scheinert, J. Dengg, A. Biastoch, and A. Funk (2006), Decadal variability of subpolar gyre transport and its reverberation in the North Atlantic overturning, *Geophys. Res. Lett.*, *33*, L21S01, doi:10.1029/2006GL026906.

Bourles, B., Y. Gouriou, and R. Chuchla (1999a), On the circulation in the upper layer of the western equatorial Atlantic, *J. Geophys. Res.*, *104*, 21,151–21,170.

Bourles, B., R. Molinari, E. Johns, W. Wilson, and K. Leaman (1999b), Upper layer currents in the western tropical North Atlantic (1989–1991), *J. Geophys. Res.*, *104*, 1361–1375.

Boyer, T., and S. Levitus (1997), *Objective Analyses of Temperature and Salinity for the World Ocean on a 1/4 Degree Grid*, *NOAA Atlas NESDIS*, vol. 11, 62 pp., NOAA, Silver Spring, Md.

Brandt, P., F. Schott, C. Provost, A. Kartavtseff, V. Hormann, B. Bourles, and J. Fischer (2006), Circulation in the central equatorial Atlantic: Mean and intraseasonal to seasonal variability, *Geophys. Res. Lett.*, *33*, L07609, doi:10.1029/2005GL025498.

Brandt, P., V. Hormann, B. Bourles, J. Fischer, F. Schott, L. Stramma, and M. Dengler (2008), Oxygen tongues and zonal currents in the equatorial Atlantic, *J. Geophys. Res.*, *113*, C04012, doi:10.1029/2007JC004435.

Brauch, J., and R. Gerdes (2005), Response of the northern North Atlantic and Arctic oceans to a sudden change of the North Atlantic Oscillation, *J. Geophys. Res.*, *110*, C11018, doi:10.1029/2004JC002436.

Cherubin, L., and P. Richardson (2007), Caribbean current variability and the influence of the Amazon and Orinoco freshwater plumes, *Deep Sea Res., Part I*, *54*, 1451–1473, doi:10.1016/j.dsr.2007.04.021.

Curry, R. (2001), HydroBase 2: A database of hydrographic profiles and tools for climatological analysis, technical report, Woods Hole Oceanogr. Inst., Woods Hole, Mass.

Dengg, J., C. Böning, U. Ernst, R. Redler, and A. Beckmann (1999), Effects of an improved model representation of overflow water on the subpolar North Atlantic, *Int. World Ocean Circ. Exp. Newsl.*, *37*, 10–15.

Eden, C., and C. Böning (2002), Sources of eddy kinetic energy in the Labrador Sea, *J. Phys. Oceanogr.*, *32*, 3346–3363.

Fratantoni, D., and D. Glickson (2002), North Brazil Current Ring generation and evolution observed with SeaWiFS, *J. Phys. Oceanogr.*, *32*, 1058–1074.

Fratantoni, D., and P. Richardson (2006), The evolution and demise of North Brazil Current rings, *J. Phys. Oceanogr.*, *36*, 1241–1264.

Fratantoni, D., W. Johns, T. Townsend, and H. Hurlburt (2000), Low-latitude circulation and mass transport pathways in a model of the tropical Atlantic Ocean, *J. Phys. Oceanogr.*, *30*, 1944–1966.

Garzoli, S., A. Ffield, and Q. Yao (2003), North Brazil Current rings and the variability in the latitude of retroflection, in *Interhemispheric Water Exchange in the Atlantic Ocean*, edited by G. Goni and P. Malanotte-Rizzoli, *Elsevier Oceanogr. Ser.*, *68*, 357–374.

Goes, M., R. Molinari, I. da Silveira, and I. Wainer (2005), Retroflections of the North Brazil Current during February 2002, *Deep Sea Res., Part I*, *52*, 647–667, doi:10.1016/j.dsr.2004.10.010.

Goni, G., and W. Johns (2003), Synoptic study of warm rings in the North Brazil Current retroflection region using satellite altimetry, in *Interhemispheric Water Exchange in the Atlantic Ocean*, edited by G. Goni and P. Malanotte-Rizzoli, *Elsevier Oceanogr. Ser.*, *68*, 335–356.

Hellweger, F., and A. Gordon (2002), Tracing Amazon River water into the Caribbean Sea, *J. Mar. Res.*, *60*, 537–549.

Hüttl, S., and C. Böning (2006), Mechanisms of decadal variability in the shallow subtropical-tropical circulation of the Atlantic Ocean: A model study, *J. Geophys. Res.*, *111*, C07011, doi:10.1029/2005JC003414.

Hüttl-Kabus, S., and C. Böning (2008), Pathways and variability of the off-equatorial undercurrents in the Atlantic Ocean, *J. Geophys. Res.*, *113*, C10018, doi:10.1029/2007JC004700.

Jochum, M., and P. Malanotte-Rizzoli (2003), On the generation of North Brazil Current rings, *J. Mar. Res.*, *61*, 147–173.

Johns, W., T. Lee, F. Schott, R. Zantopp, and R. Evans (1990), The North Brazil Current retroflection: Seasonal structure and eddy variability, *J. Geophys. Res.*, *95*, 22,103–22,120.

Kirchner, K., M. Rhein, C. Mertens, C. Böning, and S. Hüttl (2008), Observed and modeled meridional overturning circulation related flow into the Caribbean, *J. Geophys. Res.*, *113*, C03028, doi:10.1029/2007JC004320.

Klein, B., and M. Tomczak (1994), Identification of diapycnal mixing through optimum multiparameter analysis 2. Evidence for unidirectional diapycnal mixing in the front between North and South Atlantic Central Water, *J. Geophys. Res.*, *99*, 25,275–25,280.

Kraus, E., and J. Turner (1967), A one-dimensional model of the seasonal thermocline I. A laboratory experiment and its interpretation, *Tellus*, *19*, 88–97.

Levitus, S., and T. P. Boyer (1994), *World Ocean Atlas 1994*, vol. 4, *Temperature*, *NOAA Atlas NESDIS*, vol. 4, 129 pp., NOAA, Silver Spring, Md.

Mémery, L., M. Arhan, X. Alvarez-Salgado, M. Messias, H. Mercier, C. Castro, and A. Rios (2000), The water masses along the western boundary of the south and equatorial Atlantic, *Prog. Oceanogr.*, *47*, 69–98.

Ollitrault, M., M. Lankhorst, D. Fratantoni, P. Richardson, and W. Zenk (2006), Zonal intermediate currents in the equatorial Atlantic Ocean, *Geophys. Res. Lett.*, *33*, L05605, doi:10.1029/2005GL025368.

Pacanowski, R. (1995), MOM2 documentation, users guide and reference manual, *Tech. Rep. 3*, 329 pp., Geophys. Fluid Dyn. Lab. Ocean Group, Princeton, N. J.

Rhein, M., K. Kirchner, C. Mertens, R. Steinfeldt, M. Walter, and U. Fleischmann-Wischnath (2005), Transport of South Atlantic Water through the passages south of Guadeloupe and across 16°N, 2000–2004, *Deep Sea Res., Part I*, *52*, 2234–2249.

Schmitz, W., Jr., and P. Richardson (1991), On the sources of the Florida Current, *Deep Sea Res., Part A*, *38*, suppl. 1, S379–S409.

Schott, F., and C. Böning (1991), The WOCE model in the western equatorial Atlantic: Upper layer circulation, *J. Geophys. Res.*, *96*, 6993–7004.

Schott, F., J. Fischer, and L. Stramma (1998), Transports and pathways of upper layer circulation in the western tropical Atlantic, *J. Phys. Oceanogr.*, *28*, 1904–1928.

Signorini, S., R. Murtugudde, C. McClain, J. Christian, J. Picaut, and A. Busalacchi (1999), Biological and physical signatures in the tropical and subtropical Atlantic, *J. Geophys. Res.*, *104*, 18,367–18,382.

Snowden, D., and R. Molinari (2003), Subtropical cells in the Atlantic Ocean: An observational summary, in *Interhemispheric Water Exchange in the Atlantic Ocean*, edited by G. Goni and P. Malanotte-Rizzoli, *Elsevier Oceanogr. Ser.*, *68*, 287–312.

Stramma, L., and F. Schott (1999), The mean flow field of the tropical Atlantic Ocean, *Deep Sea Res., Part II*, *46*, 279–303.

Stramma, L., J. Fischer, P. Brandt, and F. Schott (2003), Circulation, variability and near-equatorial meridional flow in the central tropical Atlantic, in *Interhemispheric Water Exchange in the Atlantic Ocean*, edited by G. Goni and P. Malanotte-Rizzoli, *Elsevier Oceanogr. Ser.*, *68*, 1–22.

Stramma, L., S. Hüttl, and J. Schafstall (2005), Water masses and currents in the upper tropical northeast Atlantic off northwest Africa, *J. Geophys. Res.*, *110*, C12006, doi:10.1029/2005JC002939.

Suga, T., and L. Talley (1995), Antarctic Intermediate Water circulation in the tropical and subtropical South Atlantic, *J. Geophys. Res.*, *100*, 13,441–13,453.

Urbano, D., R. D. Almeida, and P. Nobre (2008), Equatorial Undercurrent and North Equatorial Countercurrent at 38°W: A new perspective from direct velocity data, *J. Geophys. Res.*, *113*, C04041, doi:10.1029/2007JC004215.

Willebrand, J., B. Barnier, C. Böning, C. Dieterich, P. Killworth, C. Le Provost, Y. Jia, J.-M. Molines, and A. New (2001), Circulation characteristics in three eddy-permitting models of the North Atlantic, *Prog. Oceanogr.*, *48*, 123–161.

Wilson, W., E. Johns, and R. Molinari (1994), Upper layer circulation in the western tropical North Atlantic Ocean during August 1989, *J. Geophys. Res.*, *99*, 22,513–22,523.

Zhang, D., M. McPhaden, and W. Johns (2003), Observational evidence for flow between the subtropical and tropical Atlantic: The Atlantic subtropical cells, *J. Phys. Oceanogr.*, *33*, 1783–1797.

C. W. Böning, Leibniz Institut für Meereswissenschaften an der Universität Kiel (IFM-GEOMAR), D-24105 Kiel, Germany.

S. Hüttl-Kabus, K. Kirchner, and M. Rhein, Institut für Umweltphysik, Abteilung Ozeanographie, Universität Bremen, D-28359 Bremen, Germany. (kkirchner@uni-bremen.de)